The Mechanical Energy Budget of a Regional Ocean Model

PARKER MACCREADY

University of Washington, Seattle, Washington

SARAH N. GIDDINGS

University of California, San Diego, La Jolla, California

(Manuscript received 8 April 2016, in final form 29 June 2016)

ABSTRACT

A method is presented for calculating a complete, numerically closed, mechanical energy budget in a realistic simulation of circulation in a coastal–estuarine domain. The budget is formulated in terms of the "local" available potential energy (APE; Holliday and McIntyre 1981). The APE may be split up into two parts based on whether a water parcel has been displaced up or down relative to its rest depth. This decomposition clearly shows the different APE signatures of coastal upwelling (particles displaced up by wind) and the estuary (particles displaced down by mixing). Because the definition of APE is local in almost the same sense that kinetic energy is, this study may form meaningful integrals of reservoir and budget terms even over regions that have open boundaries. However, the choice of volume to use for calculation of the rest state is not unique and may influence the results. Complete volume-integrated energy budgets over shelf and estuary volumes in a realistic model of the northeast Pacific and Salish Sea give a new way to quantify the state of these systems and the physical forces that influence that state. On the continental shelf, upwelling may be quantified using APE, which is found to have order-one seasonal variation with an increase due to winds and decrease due to mixing. In the Salish Sea estuarine system, the APE has much less seasonal variation, and the magnitude of the most important forcing terms would take over 7 months to fully drain this energy.

1. Introduction

Energy conservation provides a useful framework for understanding fluid systems (Wunsch and Ferrari 2004; Ferrari and Wunsch 2009; Tailleux 2013) because the system state and function may be quantified using common units in terms of energy reservoirs and the fluxes between them. This has allowed, for example, estimation of the relative importance of wind, surface buoyancy fluxes, and mixing in forcing global overturning circulation (Zemskova et al. 2015). Energy has especially been useful in quantifying internal wave energy fluxes (Carter et al. 2008; Floor et al. 2011; Kang and Fringer 2012; Scotti et al. 2006) as well as mesoscale eddy fluxes (Kang and Curchitser 2015). Turbulent energy dissipation and buoyancy flux have been the focus of research efforts globally (Waterhouse et al. 2014), particularly where they may be amplified by the interaction of currents with bathymetry. Energy budgets have also been effective in the analysis of turbulent mixing (Scotti and White 2014; Winters et al. 1995).

Coastal and estuarine systems, the focus of this paper, have also been characterized in terms of energy (Biton and Gildor 2014; Cessi et al. 2014; MacCready et al. 2009), although this can be complicated because they are so strongly defined by flow through open boundaries. In addition, the presence of strong tidal currents and rough topography can lead to difficulty closing energy budgets (MacCready et al. 2009) except in cases where small perturbations are considered (Kang and Fringer 2012). In this paper, we develop a method for calculating numerically closed energy budgets using an increasingly popular definition of the available potential energy (APE) that is well defined even for regions with flow through open boundaries. The resulting budget allows us to quantify the time-varying APE that characterizes coastal upwelling on the continental shelf, along with the

Denotes Open Access content.

Corresponding author address: Parker MacCready, University of Washington, P.O. Box 355351, Seattle, WA 98195-5351.
E-mail: pmacc@uw.edu

DOI: 10.1175/JPO-D-16-0086.1

effect of wind and mixing on this reservoir. The results for the estuarine exchange flow of the adjacent Salish Sea, however, are much less conclusive. The inland waters hold a large and relatively invariant store of APE, but the dynamical balances that control it are difficult to isolate.

2. Theoretical development

Here, we derive conservation equations for kinetic energy (KE) and available potential energy for a rotating, stratified fluid. The rotating, Boussinesq, Reynolds-averaged equations of momentum, potential temperature, salinity, density, and mass conservation may be written as

$$\frac{D\mathbf{u}}{Dt} + f\hat{\mathbf{k}} \times \mathbf{u} = -\frac{1}{\rho_0}\nabla p - \frac{\hat{\mathbf{k}} g \rho}{\rho_0} + \dot{\mathbf{u}}. \tag{1}$$

$$\frac{D\theta}{Dt} = \dot{\theta}, \quad \frac{Ds}{Dt} = \dot{s}, \tag{2}$$

$$\frac{D\rho}{Dt} = \dot{\rho}, \quad \text{and} \tag{3}$$

$$\nabla \cdot \mathbf{u} = 0. \tag{4}$$

Here, D/Dt is the material derivative, $\mathbf{u}$ is the velocity, f is the Coriolis frequency, $\hat{\mathbf{k}}$ is the vertical unit vector, p is the pressure, $\rho_0 = 1023.7\,\mathrm{kg\,m^{-3}}$ is a constant background density, g is gravity, and the dot over $\dot{\mathbf{u}}$ represents all viscous and turbulent processes. The same dot notation represents all diffusive and turbulent processes in the tracer equations (2) and (3). Equation (3) for the evolution of density ρ formally comes from (2) combined with an equation of state in which density varies linearly with salinity s and potential temperature θ. We assume, for simplicity, that density is not a function of pressure and discuss consequences of this simplification later. The fluid is assumed incompressible [(4)], consistent with the Boussinesq approximation and the treatment of volume conservation in the model, the Regional Ocean Modeling System (ROMS; Haidvogel et al. 2000; Shchepetkin and McWilliams 2005). The kinetic and available potential energy per unit volume (denoted by subscript V) are defined as

$$\mathrm{KE}_V = \frac{1}{2}\rho_0 \mathbf{u} \cdot \mathbf{u}, \tag{5}$$

$$\mathrm{APE}_V = g \int_{z_*}^{z} [\rho - \rho_*(z')]\, dz'. \tag{6}$$

The definition of KE_V is standard for Boussinesq flow. The definition of APE_V (Holliday and McIntyre 1981) relies on a flattened stratification $\rho_*(z, t)$ in which all the fluid in the volume of the model domain at any instant is rearranged adiabatically to a stable, horizontally uniform rest state (Winters et al. 1995). A graphical form of the integral in (6) is shown in Fig. 1. The associated flattened state is shown in Fig. 2. Examples of the APE_V and its vertical integral from the numerical model used in this paper are shown in Fig. 3. The flattened state may change over time due to mixing and advection through open boundaries. One interpretation of the APE_V is that it is the work one would have to do against buoyancy to raise a fluid parcel of density ρ, assumed constant in the integral in (6), through a stratification $\rho_*(z)$ from its initial vertical position z_* to its current position z. This definition is local in the sense that it assigns a positive-definite potential energy to each water parcel, like the kinetic energy. In situations where disturbed isopycnals slump toward the flattened state, APE_V is typically converted to KE_V at some other location, transmitted by pressure work. Physically the APE_V field can be interpreted as indicating where potential energy will come from, not where it will appear when converted to KE. The application of (6) near the free surface requires some extra care, but in the end gives results consistent with the shallow-water energy equation, as derived below. The many benefits of this definition of available potential energy are discussed in more detail in a number of recent papers (Kang and Fringer 2010, 2012;

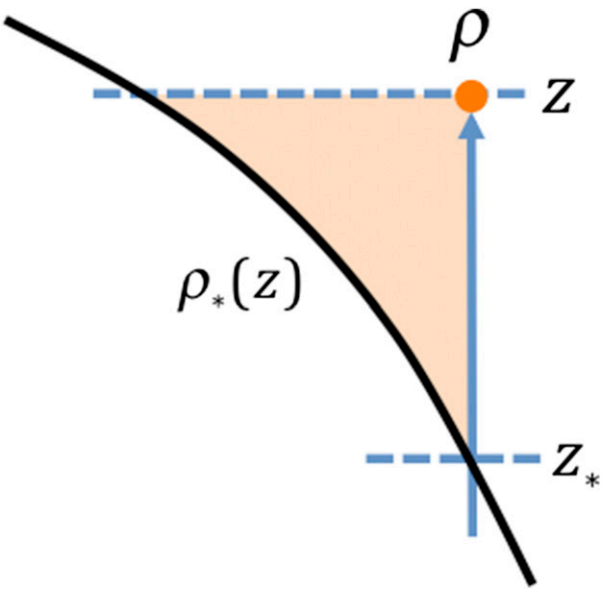

FIG. 1. Definition sketch for the calculation of available potential energy. The APE is calculated as the integral of the work done against buoyancy to move a water parcel through the flattened stratification $\rho_*(z)$. The parcel density is assumed constant during the vertical translation from its rest position z_* to its in situ position z. The APE is proportional to the area of the beige triangle in the diagram. In this visual example, the parcel has been displaced upwards relative to its rest depth so it would lead to $\mathrm{APE}_{\mathrm{up}}$.

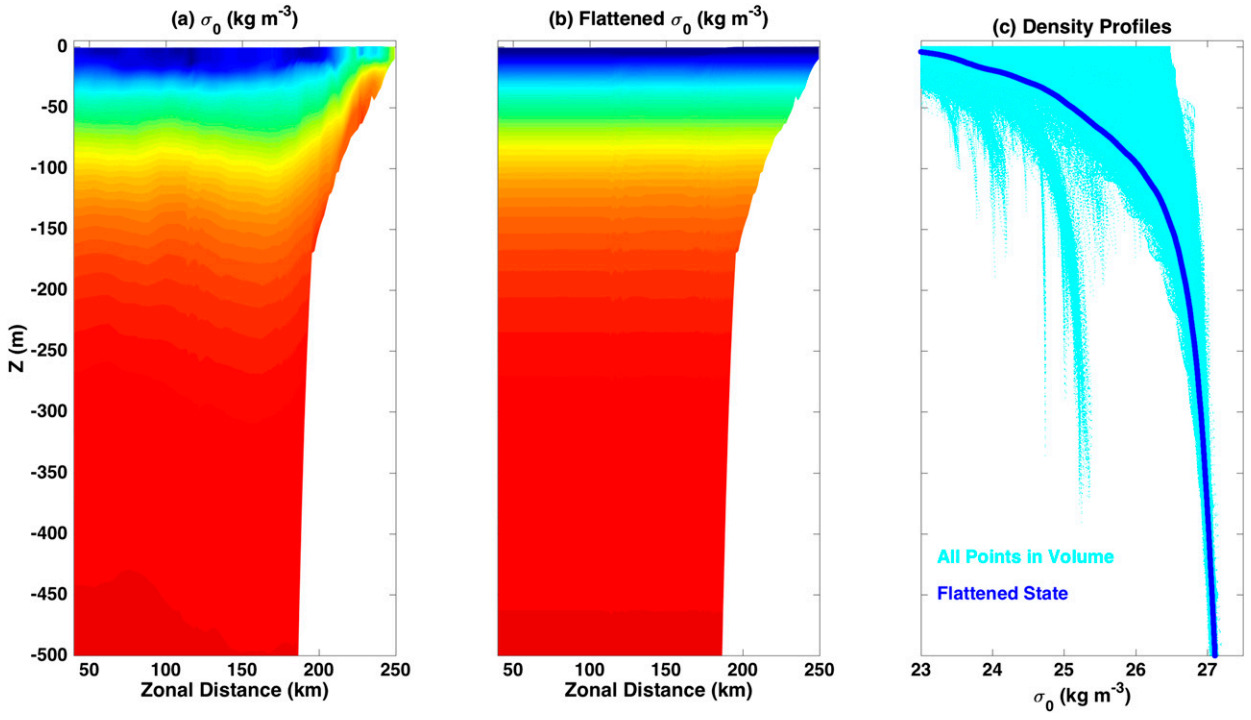

FIG. 2. (a) Instantaneous zonal section at 47°N of potential density from the model on 20 July 2005, during a time of upwelling winds. (b) Flattened density field $\rho_*(z, t)$ on the same section. (c) Potential density vs depth for all points in the domain (cyan dots) and for the flattened state (blue line). The spur of low-density values is associated with relatively freshwater in the Salish Sea. The Salish Sea is not crossed by the section in (a) and (b), but it is part of the volume used for (c).

Winters and Barkan 2013; Scotti and White 2014). In particular, the volume integral of APE_V can be shown (Winters and Barkan 2013) to be equal to the classical (Lorenz 1955), volume-integrated definition of APE.

The rest state used to calculate APE_V depends on all the fluid in the volume over which is it calculated, and in this sense it is not a purely local quantity. More importantly, it is not uniquely defined but rather depends on the choice of volume. Here, we have used the entire model domain, excluding nudging regions near the open boundaries (Fig. 3a), and so the background state is dominated by ocean properties beyond the shelf break. The motivation for this choice is that we assume motion resulting from release of APE_V on the shelf and inland waters would not extend meaningfully beyond this boundary in a time shorter than that of natural variation of the system. While this criterion is both hypothetical and qualitative, experiments using smaller volumes showed that the maximum value of APE_V decreased by only a few percent as long as some part of the volume extended beyond the shelf break.

To form an equation for the evolution of APE_V, it helps to rewrite (6) as

$$\mathrm{APE}_V = g(z - z_*)\rho - g\int_{z_*}^{z} \rho_*(z')\,dz' = g(z - z_*)\rho - F. \tag{7}$$

We have made use of the fact that ρ is a constant in the integral, and we have defined a function $F(z, z_*, t)$. This definition may seem at first to be costly to calculate for a full 3D domain, but it can be done efficiently by exploiting the fact that F may be expressed as the difference of two vertical definite integrals of ρ_* and then calculating the vector that gives this integral for any z. Taking the material derivative of APE_V, we find

$$\frac{D}{Dt}\mathrm{APE}_V = g(z - z_*)\dot{\rho} + g(\rho - \rho_*)w - g\int_{z_*}^{z} \rho_{*_t}\,dz', \quad \text{or}$$

$$\underbrace{\frac{\partial}{\partial t}\mathrm{APE}_V}_{\text{APE Storage}} = \underbrace{[-\mathbf{u}\cdot\nabla\mathrm{APE}_V + g(\rho - \rho_*)w]}_{\text{Advection+Conversion}} + \underbrace{g(z - z_*)\dot{\rho}}_{\text{Mixing}} \quad \underbrace{-\dot{F}}_{\text{Background}} \tag{8}$$

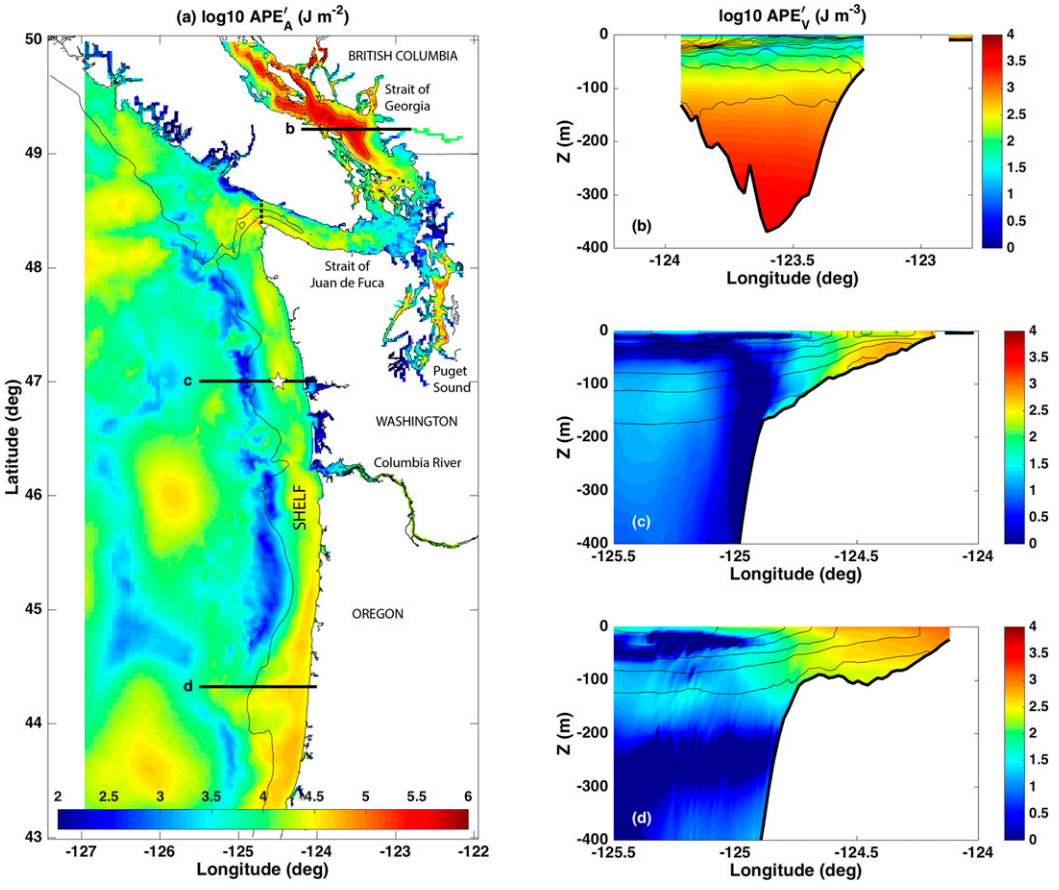

FIG. 3. (a) Map view of APE'_A (the prime means that we remove the contribution of surface height). The entire model domain is shown, and regions on the west and south where nudging is applied are blanked out. The shelf break is shown by a black contour at the 200-m isobath. (b),(c),(d) Zonal sections, taken on the three corresponding black lines of the map, showing the vertical structure of APE'_V, with potential density contours every 0.5 kg m^{-3}. This is on 20 Jul 2005, during a time of upwelling winds, as marked in Fig. 8.

Here, $\dot{F} \equiv g\int_{z_*}^{z} \rho_{*t}\, dz'$, subscript t denotes a partial derivative, and we have made use of the fact that $D\rho_*/Dt = \rho_{*t}$ because the flattened stratification is a derived field that cannot be advected. The terms in (8) look somewhat familiar to what we would find in a more standard derivation of an evolution equation for potential energy $\mathrm{PE}_V = \rho g z$, where $\rho g w$ would appear on the RHS and eventually cancel with a corresponding conversion term in the KE_V equation. We will take this into account when forming the equation for kinetic energy. We have put the RHS terms in (8) into three categories: (i) advection + conversion, (ii) mixing, and (iii) background. This formalism will carry over into the categories we use in our model-based budget.

The equation for KE_V is formed by taking the dot product of $\rho_0 \mathbf{u}$ with (1). To this we add plus and minus $\rho_* g w$ to the RHS, yielding

$$\frac{D}{Dt}\mathrm{KE}_V = -\mathbf{u}\cdot\nabla p - \rho_* g w - g(\rho-\rho_*)w + \rho_0 \mathbf{u}\cdot\dot{\mathbf{u}}, \quad \text{or}$$
$$\underbrace{\frac{\partial}{\partial t}\mathrm{KE}_V}_{\text{KE Storage}} = \underbrace{[-\mathbf{u}\cdot\nabla \mathrm{KE}_V - \mathbf{u}\cdot\nabla P - g(\rho-\rho_*)w]}_{\text{Advection+Pressure Work-Conversion}} + \underbrace{\rho_0 \mathbf{u}\cdot\dot{\mathbf{u}}}_{\text{Dissipation}}, \tag{9}$$

where we have defined a modified pressure field that satisfies $\nabla P = \nabla p + \hat{\mathbf{k}} g \rho_*$. Here, the RHS terms are put into two categories. The dissipation term may be positive (e.g., when wind forcing is

strong) or negative (e.g., when bottom friction is important).

Adding the two energy equations gives the full equation

$$\frac{D}{Dt}(\mathrm{KE}_V + \mathrm{APE}_V) = -\nabla\cdot(\mathbf{u}P) + \rho_0\mathbf{u}\cdot\dot{\mathbf{u}} + g(z-z_*)\dot{\rho} - \dot{F}, \quad \text{or}$$

$$\underbrace{\frac{\partial}{\partial t}(\mathrm{KE}_V + \mathrm{APE}_V)}_{\text{Storage}} = \underbrace{-\nabla\cdot(\mathbf{u}B)}_{\text{Bernoulli}} + \underbrace{\rho_0\mathbf{u}\cdot\dot{\mathbf{u}}}_{\text{Dissipation}} + \underbrace{g(z-z_*)\dot{\rho}}_{\text{Mixing}} \underbrace{-\dot{F}}_{\text{Background}}. \tag{10}$$

We have defined a modified Bernoulli function $B \equiv \mathrm{KE}_V + \mathrm{APE}_V + P$. Thus, the rate of change of the full energy at a point is governed by divergence of the advection of the modified Bernoulli function, the dissipation, the mixing, and the rate of change of the flattened background state.

The realistic regional simulations we are using have tides, and these can dominate the energy fields, especially in shallow waters, potentially obscuring the more important tidally averaged fields (e.g., we would like to distinguish the APE of tilted isopycnals in coastal upwelling from that of tidal surface height). To facilitate this distinction we will subtract out terms calculated using the shallow-water energy equations. The shallow-water (vertically averaged or integrated) momentum and volume conservation equations are

$$\mathbf{U}_t + \mathbf{U}\cdot\nabla_H\mathbf{U} + f\hat{\mathbf{k}}\times\mathbf{U} = -g\nabla_H\eta + \dot{\mathbf{U}}, \quad \text{and}$$
$$\eta_t + \nabla_H\cdot(H\mathbf{U}) = 0. \tag{11}$$

Here, $\mathbf{U} = (U, V)$ is the depth-averaged velocity, $\nabla_H = (\partial/\partial x, \partial/\partial y)$, η is the free surface height, $H = h + \eta$, and h is the bottom depth. Wind and bottom stress contribute to the frictional term $\dot{\mathbf{U}}$. The shallow-water, vertically integrated, kinetic and available potential energy (defined relative to a rest state with $\eta = 0$) are

$$\mathrm{KE}_A^{\mathrm{SW}} = (1/2)\rho_0 H\mathbf{U}^2, \quad \text{and}$$
$$\mathrm{APE}_A^{\mathrm{SW}} = (1/2)\rho_0 g\eta^2, \tag{12}$$

where the subscript A stands for per unit area. The shallow-water energy equation is easily derived from (11) using standard methods, yielding

$$\frac{\partial}{\partial t}(\mathrm{KE}_A^{\mathrm{SW}} + \mathrm{APE}_A^{\mathrm{SW}}) = -\nabla_H\cdot[\mathbf{U}(\mathrm{KE}_A^{\mathrm{SW}} + g\rho_0\eta H)] + \rho_0 H\mathbf{U}\cdot\dot{\mathbf{U}}. \tag{13}$$

By subtracting this from the depth-integrated full energy budget, we arrive at energy terms associated with (i) the velocity shear and (ii) the density structure.

In much of the analysis below we will be considering vertical integrals of the terms in (8) and (10), because this substantially collapses the size of the results, while retaining information specific to different horizontal locations. When taking the vertical integral of APE_V over the water column, it can be split into two parts. For water parcels over most of the water column, the meaning of (7) is clear. However, near the free surface, for the case when $\eta > 0$, we are conceptually pushing water parcels up through air, and so $\rho - \rho_* \cong \rho_0$ (because $\rho_* \cong 0$ for air). In this case, (7) may be integrated directly to give $\mathrm{APE}_V^{\mathrm{SW}} = \rho_0 gz$, and this is valid only over the interval $0 \le z \le \eta$. For the case when $\eta < 0$, we are conceptually pushing air parcels down through water, so $\rho - \rho_* \cong -\rho_0$ and hence $\mathrm{APE}_V^{\mathrm{SW}} = -\rho_0 gz$, valid over the interval $\eta \le z \le 0$. Integrating either of these vertically over the interval on which they are defined gives the expression for $\mathrm{APE}_A^{\mathrm{SW}}$ defined in (12). Thus, when taking vertical integrals of APE_V or its budget terms, we will split them into two parts, which we refer to as "internal" (denoted by a prime) and "shallow water" (denoted by SW):

$$\mathrm{APE}_A \cong \int_{-h}^{0} \mathrm{APE}_V\, dz + \frac{1}{2}\rho_0 g\eta^2 = \mathrm{APE}_A' + \mathrm{APE}_A^{\mathrm{SW}}. \tag{14}$$

In practice, when we calculate APE_A', we artificially assume that all grid cells have the size and vertical position they would have for $\eta = 0$. The KE may split up by subtracting the shallow-water terms from the full vertical integral terms. The details of the how the integrals are evaluated numerically are given in the next section.

3. Exact budget in a numerical model

Despite the fact that modeled fields are completely known, it can still be challenging to form an energy budget from them. Time differencing of saved model fields may not give accurate rates of change, and flux divergences calculated from the spatial grid are subject

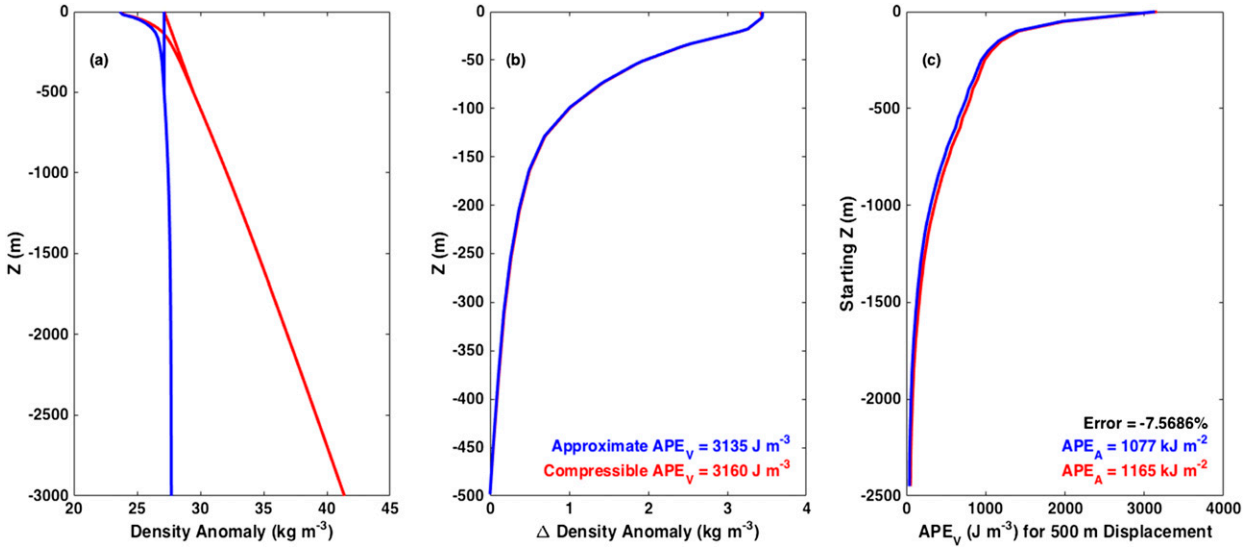

FIG. 4. Calculating APE with and without compressibility. (a) Density profiles from a deep-water location in the model (taken here as ρ_*). The red curve includes compressibility, and the blue is potential density relative to the surface. The straight lines near the top show the density following a water parcel raised from 500 m to the surface. (b) The density difference $\rho - \rho_*$ over the top 500 m for that parcel with (red) and without (blue) compressibility. The density difference, and the APE_V of the parcel, are very similar in both cases, despite the large effect of compressibility on density. (c) Profiles of APE_V calculated for parcels every 50 m, assuming they are displaced 500 m upward from their rest position, again for compressible and incompressible cases. The uppermost point on these curves corresponds to the vertical integral shown as text in (b). The water column vertical integral of the two curves in (c) gives APE'_A, shown as text. Even for these large displacements, the net error is just 8%.

to errors from differencing methods as well. Perfect volume conservation must be ensured as well (MacCready et al. 2009). In addition, the model numerical formulation may not be energy conserving (Marsaleix et al. 2008). Here, we are able to circumvent most of these problems by utilizing the "diagnostics" and "averages" available as standard ROMS output, along with hourly "history" fields of instantaneous velocity, surface height, and water properties. The diagnostics are a record of all the terms contributing to the rate of change of a property in a given grid cell, averaged over the hour between the history saves. The averages give averages of all fields over the hour (as opposed to the snapshots at the hour boundaries from the history files). The most important field from the averages for our purposes is the volume flux through grid cell boundaries, which exactly conserves volume.

ROMS uses a C grid in the horizontal, with a fixed number of terrain-following coordinates in the vertical. Our simulations (Giddings et al. 2014) use a spherical Cartesian grid and 40 vertical levels. Tracers are reported on cell centers, and velocities and turbulent fluxes on cell boundaries.

In the KE_A budget, because vertical velocities are much smaller than horizontal, we neglect them for the purpose of calculating the KE, so numerically the vertically integrated KE rate of change is

$$\frac{\partial}{\partial t}\mathrm{KE}_A \cong \frac{\partial}{\partial t}\int_{-h}^{\eta}\frac{1}{2}\rho_0(u^2+v^2)\,dz = \sum_{i=1}^{N}\left[\delta_i\frac{1}{2}\rho_0(u_i^2+v_i^2)\right]_t, \tag{15}$$

where there are N vertical layers with thickness δ_i (variable in space and time). In the following, we will drop the subscript i and just focus on the u part of the KE budget. Eventually, we interpolate horizontally to grid-box centers when adding u and v parts. The u-momentum diagnostics are reported as the balance

$$\text{u\_accel} = \text{u\_xadv} + \text{u\_yadv} + \text{u\_vadv} + \text{u\_cor} + \text{u\_prsgrd} + \text{u\_vvisc}. \tag{16}$$

The exact numerical definition of these terms involves the layer thickness, for example, $\text{u\_accel} = \langle(\delta u)_t\rangle/\langle\delta\rangle$, and $\langle\,\rangle$ denotes averaging over the time interval of the diagnostics, an hour in this case (we will omit these brackets for the remainder of the derivation). Since the free surface is moving, δ changes over time, and so $\text{u\_accel} \neq u_t$. The standard way to form the rate of change of KE is $\rho_0 u u_t = [(1/2)\rho_0 u^2]_t$ and thus involves multiplying a momentum balance term by a velocity. The velocity we use is that calculated from the volume-conserving flux Huon, reported in the averages, $\text{Huon} = DY \times \delta \times u$, for a cell

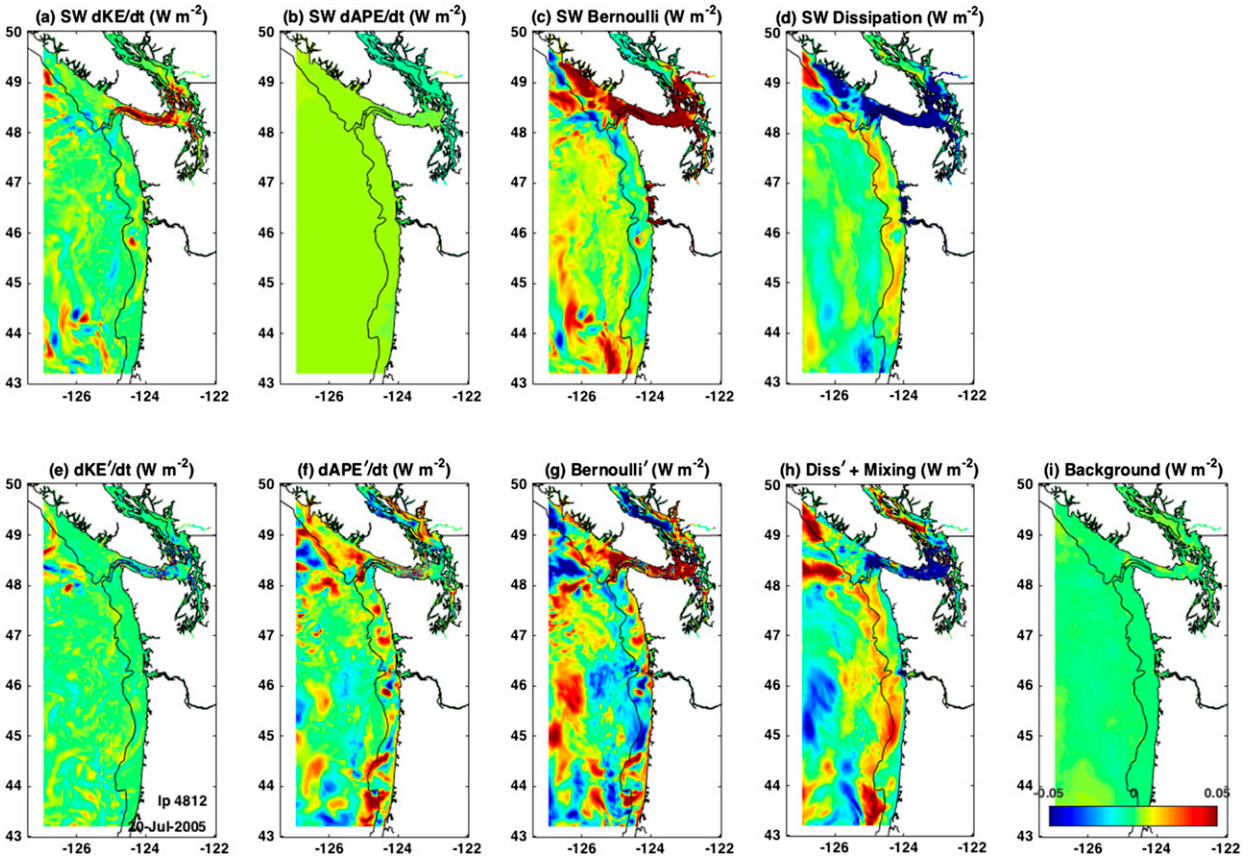

FIG. 5. Terms from the vertically integrated, tidally averaged energy budgets on 20 Jul 2005. Shallow-water terms are shown in the top row, and those from the internal budget (full minus shallow water) are shown below. The x and y axes are longitude and latitude in degrees in this and subsequent figures.

boundary of width DY in the y direction. Thus, we may show (after some manipulation) that

$$\left(\delta\frac{1}{2}u^2\right)_t = \frac{\text{Huon}}{DY}\text{u\_accel} - \delta_t\left(\frac{1}{2}u^2\right). \tag{17}$$

This is one of the terms needed to form KE_{At} in (15). This procedure then provides a template that we apply to all the diagnostics in order to arrive at a numerical budget that balances exactly (to within machine roundoff error). This does not, however, guarantee that energy is truly conserved because the model numerical scheme may not conserve energy (Marsaleix et al. 2008). Below, we quantify this error by comparing the rate of change calculated two different ways. The u part of the budget is thus

$$\underbrace{\sum\left[\rho_0\left(\frac{\text{Huon}}{DY}\text{u\_accel}\right) - \delta_t\frac{1}{2}\rho_0 u^2\right]}_{\text{KE Storage}} = \underbrace{\sum\left(\rho_0\left\{\frac{\text{Huon}}{DY}[\text{u\_}(x,y,v)\text{adv} + \text{u\_cor} + \text{u\_prsgrd}]\right\} - \delta_t\frac{1}{2}\rho_0 u^2\right)}_{\text{Advection+Pressure Work-Conversion}} + \underbrace{\sum\left[\rho_0\left(\frac{\text{Huon}}{DY}\text{u\_vvisc}\right)\right]}_{\text{Dissipation}}. \tag{18}$$

The full KE_A budget is formed by interpolating this to grid cell centers and adding it to the corresponding v part of the budget. We have grouped the terms into the same categories used in the analytical expression [(9)], in particular combining the advection and pressure work terms. By doing this we are able to completely neglect explicit calculation of terms from the (hydrostatic) z-momentum balance because they cancel exactly (and so

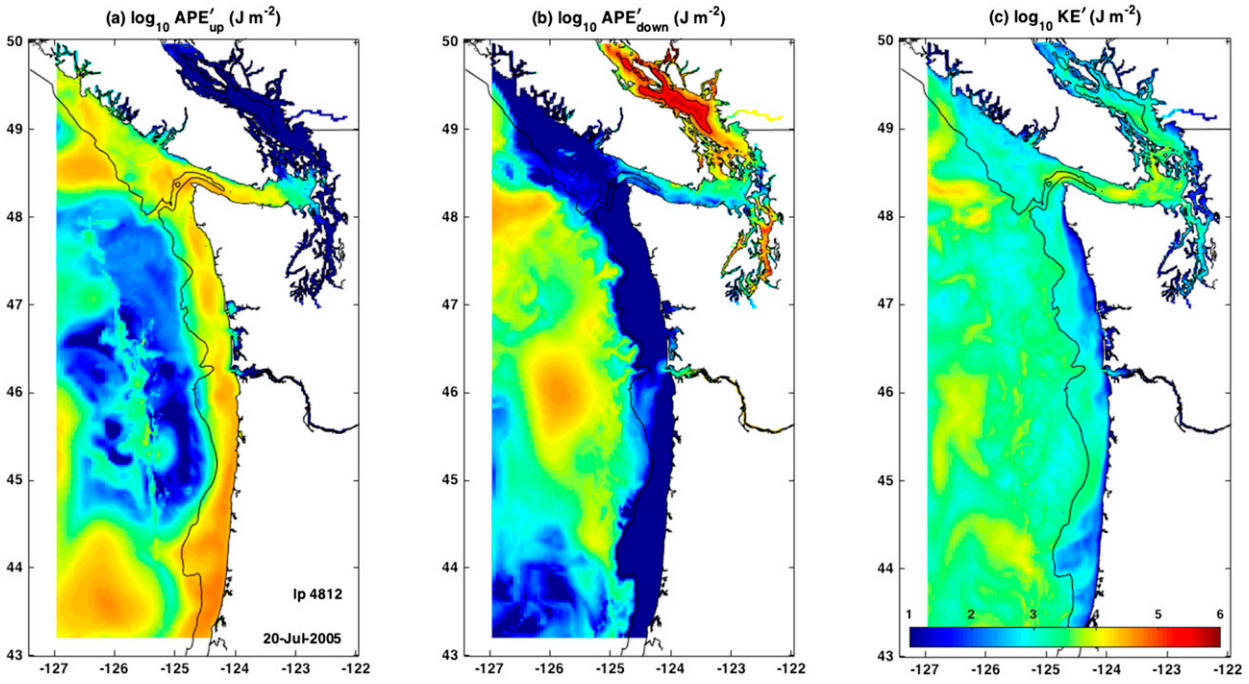

FIG. 6. Tidally averaged APE'_A on 20 Jul 2005, associated with (a) upward displacement of water parcels away from the flattened state and (b) those displaced downward. This is during a time of upwelling, and the APE on the shelf is mostly "up," whereas in the Salish Sea it is mostly "down." Mesoscale eddies are apparent beyond the shelf break with both signs of APE'_A. (c)The internal KE′.

the conversion term does not appear explicitly). The Coriolis term formally drops out of the analytical version but is retained here to avoid small numerical imbalances. The term $\delta_t(1/2)\rho_0 u^2$ that was subtracted from the storage term on the LHS (in order to account for the way changing cell thickness is embedded in the diagnostics) is also subtracted from the advection term on the RHS, the category into which it naturally falls.

The APE'_A budget is calculated using similar methods but requires some extra attention to the equation of state. The numerical form will be

$$\frac{\partial}{\partial t}\mathrm{APE}'_A = \sum \delta_*(\mathrm{APE}_V)_t. \tag{19}$$

Here, δ_* is the layer thickness calculated with $\eta = 0$. We may write the time derivative in (19) as

$$\frac{\partial}{\partial t}\mathrm{APE}_V = g(z - z_*)\rho_t - g\int_{z_*}^{z} \rho_{*t}\, dz'. \tag{20}$$

Assuming a locally linear equation of state, we may write

$$\frac{1}{\rho}\rho_t = -\alpha\theta_t + \beta s_t, \quad \text{where} \quad \alpha = -\rho^{-1}\partial\rho/\partial\theta \quad \text{and}$$
$$\beta = \rho^{-1}\partial\rho/\partial s. \tag{21}$$

A similar approach was presented in Zemskova et al. (2015). The diagnostics for potential temperature and salinity are similar to those reported for velocity; for example, for salinity they are

$$\text{salt\_rate} = \text{salt\_}(x, y, \upsilon)\text{adv} + \text{salt\_}(h, \upsilon)\text{diff}. \tag{22}$$

The rate is defined in a similar way to the acceleration term from the momentum equation salt_rate $= (\delta s)_t/\delta$. The ROMS equation of state used in our simulations includes compressibility in the calculation of density for the purposes of calculating pressure gradients while imposing incompressibility for volume conservation. We use the ROMS compressible equation of state to calculate α and β in each grid box at each time; however, when we calculate the APE_V itself, we use the potential density referenced to zero pressure, which is consistent with keeping the parcel density constant in the integral (6). We also use potential density in place of density when forming ρ_* at each time step. This simplifies the calculation but introduces some intrinsic error in the sense that the integral (6) with compressibility will be somewhat different than that calculated with potential density. In principle, this may not be a large problem because compressibility will affect both ρ and ρ_* similarly over the integral (6), and so their difference will be little changed. Experiments

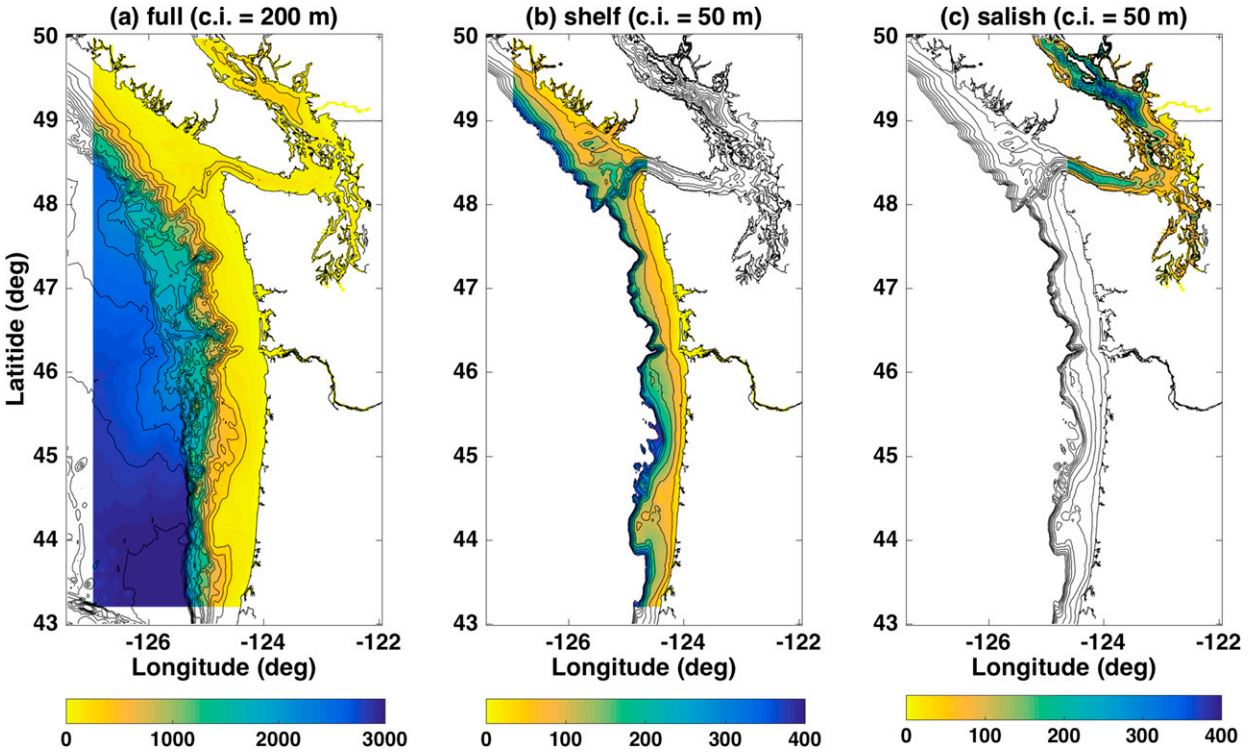

FIG. 7. Regions of integration used in the volume integrals. (a) The full domain. (b) The shelf domain extends seaward to the 400-m isobath, and (c) the Salish Sea domain extends to 124.625°W in the Strait of Juan de Fuca. Color indicates depth; note change of color scale between panels.

doing the calculation both ways (Fig. 4) showed that the error in the calculation of APE_V was less than 8% even for 500-m displacements. Young (2010) discusses this more, and Saenz et al. (2015) show how to calculate ρ_* efficiently even for compressible fluids. We choose to stick with the incompressible form for the energy budget because it simplifies the calculation significantly without losing the fundamental balances. Using (19) through (22), we may write the full APE'_A budget as

$$\underbrace{\sum\delta_*\left\{g(z-z_*)\rho\left[-\alpha\mathrm{temp\_rate}+\beta\mathrm{salt\_rate}+\frac{\delta_t}{\delta}(\alpha\theta-\beta s)\right]-g\int_{z_*}^{z}\rho_{*_t}\,dz'\right\}}_{\mathrm{APE}'\mathrm{Storage}}$$
$$=\underbrace{\sum\delta_*\left\{g(z-z_*)\rho\left[-\alpha\mathrm{temp\_}(x,y,v)\mathrm{adv}+\beta\mathrm{salt\_}(x,y,v)\mathrm{adv}+\frac{\delta_t}{\delta}(\alpha\theta-\beta s)\right]\right\}}_{\mathrm{Advection+Conversion}}$$
$$+\underbrace{\sum\delta_*\{g(z-z_*)\rho[-\alpha\mathrm{temp\_}(h,v)\mathrm{diff}+\beta\mathrm{salt\_}(h,v)\mathrm{diff}]\}}_{\mathrm{Mixing}}+\underbrace{\sum\delta_*\left\{-g\int_{z_*}^{z}\rho_{*_t}\,dz'\right\}}_{\mathrm{Background}}. \tag{23}$$

The full APE_A equation is then made by adding $\partial/\partial t[(1/2)\rho_0 g\eta^2]$ to the APE' storage term on the LHS of (23) and to the advection term on the RHS. Again the budget closes (numerically at least) by construction because the diagnostics balance.

The energy budget for the shallow-water flow [(13)] was calculated using techniques similar to those given for the KE budget, but we omit the details here because tidal energy is not the focus of this paper.

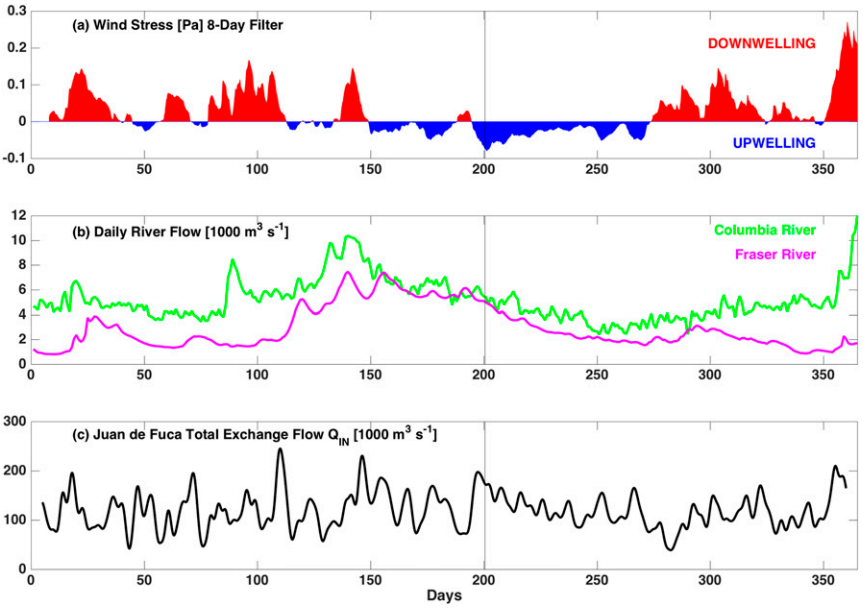

FIG. 8. Environmental time series for the 2005 simulation. (a) Wind stress from a location (star on Fig. 3a) on the shelf is filtered using an 8-day decaying exponential (Austin and Barth 2002), so negative values are expected to correspond to times when upwelled water is present on the shelf. (b) Daily river flow is plotted for the Columbia River (data from USGS) and the Fraser River (data from Environment and Climate Change Canada). (c) The strength of the inflowing part of the tidally averaged estuarine exchange flow at the mouth of the Strait of Juan de Fuca (dashed line in Fig. 3a), quantified using isohaline coordinates (MacCready 2011).

4. Results and discussion

We will explore the energy budget using a year-long realistic ROMS hindcast of the northeast Pacific and Salish Sea (a term referring to the combined inland waters of Puget Sound, Strait of Georgia, and Strait of Juan de Fuca) shown in Fig. 3. The model is optimized for shelf processes, where the grid size is 1.5 km. The same resolution in the Salish Sea means that it does a poor job of representing the inland waters but nonetheless produces an estuarine circulation with realistic magnitude and variability. The model is forced with daily ocean sea surface height, velocity, temperature, and salinity from the Navy Coastal Ocean Model (Barron et al. 2006, 2007) on the south and west boundaries, 3-hourly wind, atmospheric heat flux fields from a regional MM5 forecast model (Mass et al. 2003), daily flow of 16 rivers from the U.S. Geological Survey and Environment Canada, and eight tidal constituents from the TPXO7.2 global fields (Egbert and Erofeeva 2002). The model setup and extensive validation against moored, shipboard, satellite, and glider data are detailed in Giddings et al. (2014). Hourly model history fields were saved, along with diagnostic and average information as described above. The domain is part of an eastern boundary upwelling region, the northern part of the California Current System, and there is clear wind-driven upwelling in the spring and summer, with local and remote forcing (Hickey et al. 2006; Pierce et al. 2006).

Energy budget and reservoir terms were calculated for each hour of the year 2005, vertically integrated, and tidally averaged using a 24–24–25 Godin filter (Emery and Thomson 1998). Terms from both the shallow water and internal energy budgets on 20 July 2005 are shown in Fig. 5. Movies made from such frames are entertaining to watch but can be difficult to interpret because the terms inherently involve time and space derivatives.

The shallow-water terms show patches of positive and negative flux divergence around eddies on the shelf and deeper waters (Figs. 5a,c). The shallow-water APE_t^{SW} in Fig. 5b is much smoother and is dominated by subtidal setup or setdown of the free surface in the Salish Sea. The shallow-water dissipation terms (Fig. 5d) show persistent loss of energy in the Strait of Juan de Fuca and nearby sills, where tidal currents are 1 m s^{-1} or greater. This is balanced by a convergence of shallow-water Bernoulli function (Fig. 5c), mostly pressure work, which, when viewed as a movie, pulses with the spring–neap cycle. At other times the shallow-water dissipation terms have widespread positive values when wind stress is in the same direction as the depth-averaged flow.

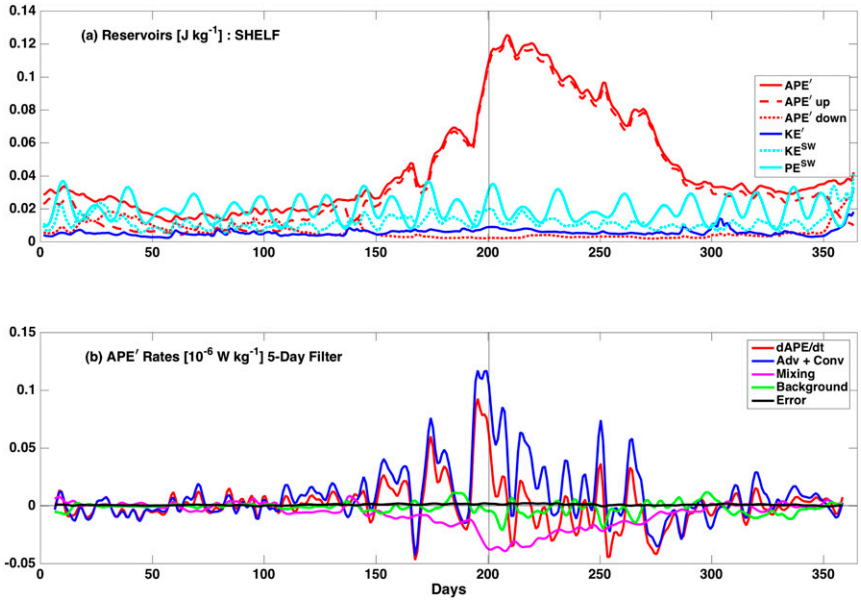

FIG. 9. (a) Volume-integrated energy terms for the shelf domain. Energy reservoir terms (divided by the mass of the volume of integration). (b) Terms from the low-passed (5-day filter) APE′ budget. The energy is dominated by APE'_{up}, which is forced by upwelling winds. This reservoir decays in the late summer and fall, despite continued upwelling winds, apparently due to the mixing term, which could indicate restratification due to heating. The vertical line is at 20 Jul 2005, the time used for all snapshot figures.

The internal energy terms are also patchy and difficult to interpret simply. The magnitude of the Bernoulli term is comparable to what was seen in the shallow-water budget, but now it is mostly balanced by the rate of change of APE′, indicating that isopycnal displacements are playing a bigger role, as would be expected for baroclinic eddies. The dissipation and mixing (Fig. 5h) are dominated by loss of energy in the Strait of Juan de Fuca and nearby sills. The background term (Fig. 5i) is smooth and not far from zero, which means that the variation of the flattened state is not a dominant player in the balance at this time.

Looking at the vertically integrated, tidally averaged, reservoir terms on the same day (Fig. 6), the energy patterns are somewhat clearer. We focus on the internal fields and plot the APE′ from the same day as in Fig. 3 but separate it into two parts by defining two types of this energy: one associated with water parcels displaced up from their rest depth APE'_{up} and one associated with those displaced down APE'_{down} (which sum to the original APE′, shown in Fig. 3). On this day, the APE'_{up} is high all along the shelf (Fig. 6a), a clear signal of upwelling. There are also signals of cold-core mesoscale eddies offshore. The APE'_{down} (Fig. 6b) reveals a warm-core eddy offshore, centered around 46°N. The biggest signal in APE'_{down} is in the Salish Sea, where the relative freshness of water retained in the deep Strait of Georgia and Puget Sound basins stores a great deal of energy (also evident in Fig. 3b). It is this potential energy that is eventually converted into the estuarine exchange flow that characterizes the subtidal circulation of this system (Sutherland et al. 2011). The kinetic energy due to the sheared part of the flow (Fig. 6c) is, in contrast, much smaller. At different times, other features are apparent, especially when windstorms drive faster currents in the nonsummer months.

The time series of volume-integrated energy reservoir and flux divergence terms may be created by taking area averages of the depth-integrated terms. In Fig. 7, we define geographic areas for the shelf (Fig. 7b) and Salish Sea (Fig. 7c). Time series of environmental terms are shown in Fig. 8. The north (N)–south (S) wind stress from a location on the shelf, averaged over the preceding 8 days using an exponentially decaying weighting function with 8-day *e*-folding time, is plotted in Fig. 8a. This particular filtered stress has been shown (Austin and Barth 2002) to be a good predictor of the presence of upwelled water below the mixed layer on the Oregon shelf, and we use it here to distinguish different aspects of the effect of wind forcing on the energy budget. The daily river flow from the two largest rivers used to force the model is plotted in Fig. 8b; the Columbia is on the shelf, and the Fraser is in the Salish Sea. The strength of the estuarine exchange flow through the Strait of Juan

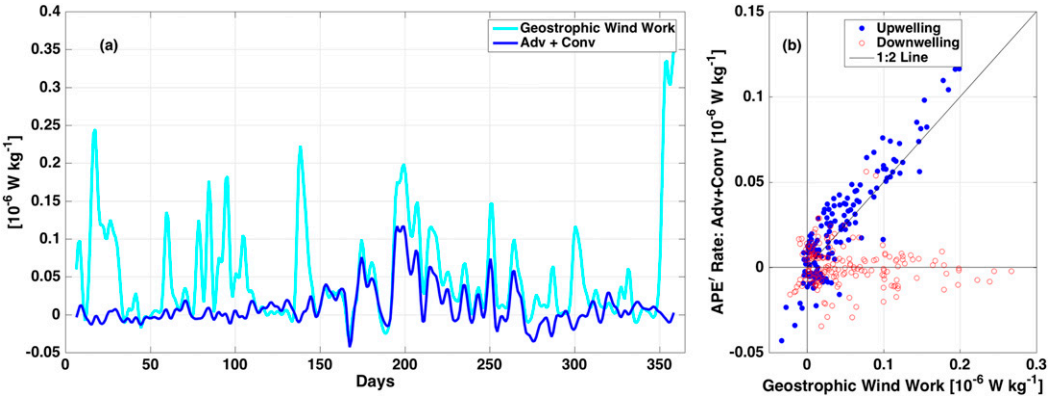

FIG. 10. (a) A time series of the shelf volume-integrated APE′ budget term advection + conversion, divided by the shelf mass (from Fig. 9b), along with the rate of geostrophic wind work over the same region. (b) A scatterplot of the same two fields, colored by the sign of the filtered wind stress from Fig. 8a. Roughly half of the work done by upwelling-favorable winds goes into the creation of APE′ by advection.

de Fuca is plotted in Fig. 8c, quantified using the tidally averaged inflowing volume flux, calculated using an isohaline coordinate system (MacCready 2011; Geyer and MacCready 2013).

Time series for terms integrated over the shelf region are presented in Fig. 9, showing (Fig. 9a) reservoir terms and (Fig. 9b) APE′ budget terms. The APE′ budget variables are the four terms

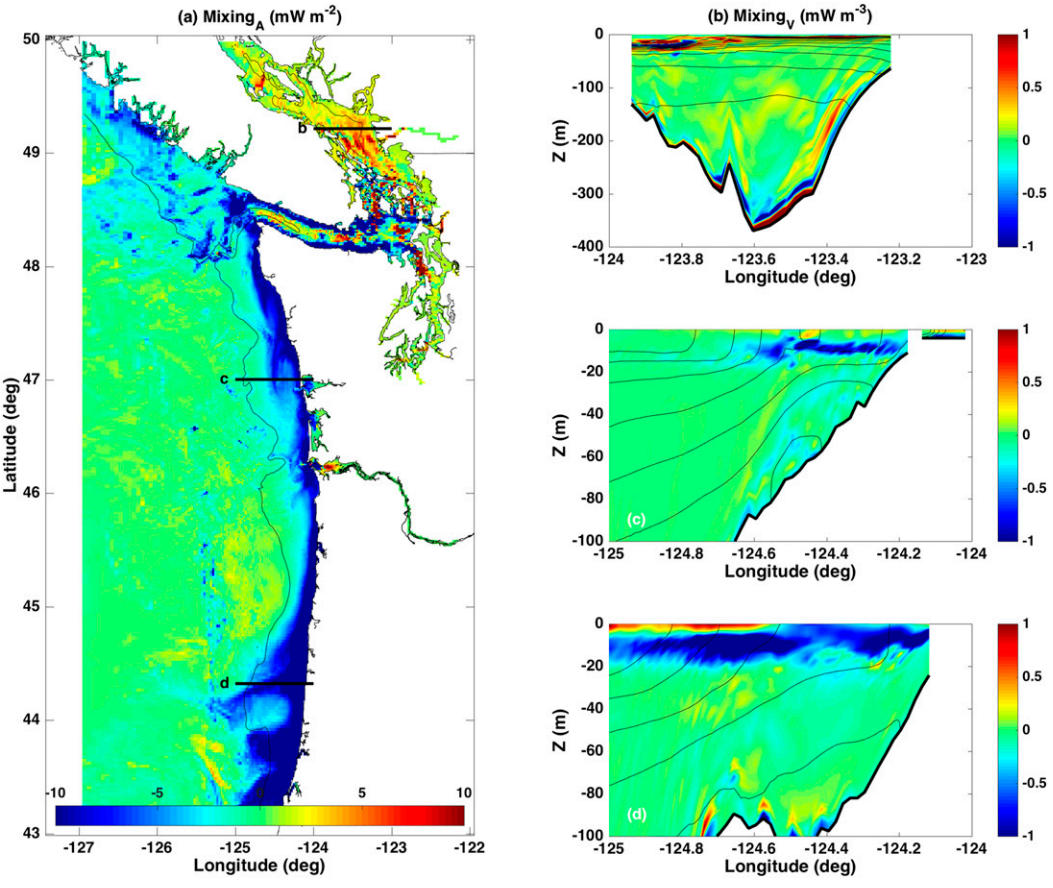

FIG. 11. The tidally averaged mixing term from the APE′ budget, from 20 Jul 2005, plotted as a (a) vertical integral and as (b),(c),(d) sections. The pervasive negative effect of mixing on APE′ is apparent on the shelf in (a), and the two shelf sections in (c) and (d) reveal the APE′ loss to be occurring near the surface, where mixing down of warm water competes with the upwelling of cold water.

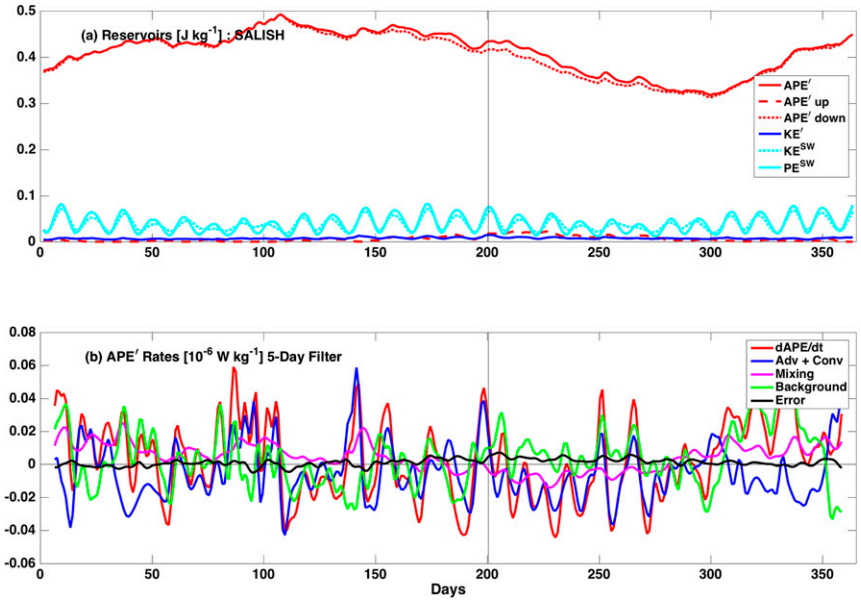

FIG. 12. (a) Volume-integrated energy terms for the Salish Sea region. Energy reservoir terms (divided by mass of the volume of integration). (b) Terms from the low-passed (5-day filtered) APE′ budget. The energy is dominated by APE'_{down}, indicative of the persistent freshness of water in the deep Strait of Georgia and Puget Sound relative to the ocean.

in (23): storage = (advection + conversion) + mixing + background. These have been smoothed in time using a 5-day Hanning window on the daily, tidally averaged terms. They have also been divided by the average mass of the volume to obtain units of watts per kilogram. The error term plotted in Fig. 9b is the difference between the storage term calculated in (23) and the same term calculated independently using centered differencing in time of the APE′ reservoir field. The reason for focusing on the APE′ equation is apparent in the reservoir fields in Fig. 9a, which are dominated by APE′ for most of the year. The budget terms show that the seasonal increase of APE′ is mostly driven by the advection + conversion term and is persistently drawn down by mixing. The background term is negligible, as is the error. Physically the advection + conversion term consists of two parts in this volume integral. The advection is due to advection of water parcels through the open boundaries of the shelf domain, mainly on the shelfbreak side [the advection term can be rewritten as a pure divergence using $\nabla\cdot\mathbf{u} = 0$ in (8), and so its volume integral may be expressed as an area integral of boundary fluxes using the Gauss's divergence theorem]. The advection term would result in increasing APE'_{up} if water parcels entered at depth with a density greater than ρ_* or left with density less than ρ_* near the surface (assuming a classic, wind-driven, upwelling, cross-shore circulation with surface Ekman transport offshore). The conversion term is positive anytime we have upward advection of water denser than ρ_*. We expect the conversion to dominate over advection because the APE′ signal is generally smaller at the shelf break than it is on the shelf (Fig. 3). We do not, however, show them separately because in (23) they are calculated together and rely on the intrinsic volume conservation that results when summing all the advective terms.

The advection + conversion term on the shelf can be explained in part as being forced by geostrophic wind work (Fig. 10). The geostrophic wind work is calculated using the horizontal pressure gradient from the model diagnostics in the uppermost bin to calculate the geostrophic velocity and then multiplying by the wind stress. The results are then time averaged in the same way as the other energy budget terms and integrated over the shelf area. Tidal and other high-frequency motions will, of course, not be in geostrophic balance, but the residual after time averaging should approximate the underlying geostrophic current. Comparing the two signals, there is clear correlation, especially during the summer (Fig. 10a). The geostrophic wind work is almost always positive and during times of upwelling winds is about twice the size of the advection + conversion budget term (Fig. 10b). The two signals are uncorrelated during downwelling winds. This factor of 2 is consistent with a simple 1.5-layer analytical model of wind-driven upwelling (Cushman-Roisin and Beckers 2011) in which the work done by the wind ends up equally partitioned between kinetic and potential energy. However, the

situation is clearly more complicated because the reservoir terms do not show equipartition (Fig. 9a).

The mixing term causes persistent decay of APE′, especially after day 200 (Fig. 9b), and this term is plotted as a vertical integral and as sections in Fig. 11. The APE′ loss due to this term is apparent on the shelf in near-surface waters (Figs. 11c,d) where surface heating is mixed down and decreases the density of water parcels that have high APE′ because of upward advection.

The energy budgets in the Salish Sea volume are plotted in Fig. 12. The reservoir terms are dominated by $\mathrm{APE}'_{\mathrm{down}}$ (Fig. 12a) and vary by about ±20% over the year, as compared to the order-one variation of APE′ we saw on the shelf. The terms influencing this (Fig. 12b) do not show any clear pattern, and all may be important in different proportion at a given time. Also there is a small but nonnegligible error in the budget when we compare the $d\mathrm{APE}'/dt$ from the budget to that calculated by time differencing the reservoir. This may be evidence of a fundamental lack of energy conservation in the underlying model. Looking at the size of terms is informative; taking $0.4\,\mathrm{J\,kg^{-1}}$ as a typical size of the APE′ reservoir and dividing by $-0.02 \times 10^{-6}\,\mathrm{W\,kg^{-1}}$ as a typical size of the loss due to advection + conversion, we arrive at a time scale of ~231 days for this term to drain all the energy from the APE′ reservoir. From this we may conclude that the APE′ reservoir is so large compared to the forcing terms that it acts as a kind of flywheel in the system, with the ability to maintain the estuarine circulation despite large variability of the forcing. Fraser River flow varies by a factor of 9 over the year, and the exchange flow as quantified by Q_{IN} varies by a similar amount but with no obvious correlation (Fig. 8). Similarly no significant correlation was found between the advection + conversion and Q_{IN} or between mixing and tides (as quantified by the reservoir term $\mathrm{KE}^{\mathrm{SW}}$). In a more idealized estuary we would expect that the energy budget would consist of mixing (a source of APE′) balancing advection + conversion (a sink of APE′), and the annual averages of these terms do match this expectation, but they are swamped by larger, short-term variability of other terms. This is consistent with previous results from a more detailed model of the Salish Sea (Sutherland et al. 2011) where the variability of exchange flow salt flux was found to be only weakly correlated with variability of wind and tides. An additional complication to interpretation of Q_{IN} is that the exchange flow through Juan de Fuca sometimes has three layers. This happens when the Columbia River plume extends into the Strait during downwelling winds (Thomson et al. 2007). The primary conclusion is only the most obvious one; the APE′ is large compared to the terms forcing it and so varies little.

5. Summary and conclusions

We have presented a method for calculating numerically closed energy budgets using stored output from ROMS simulations. By using a local definition of the available potential energy, such budgets may be analyzed in localized regions, and we chose specific examples of the continental shelf and the Salish Sea. While complete budgets for KE and APE may be formed, we find that the most informative budget is for APE′, defined as the APE associated with the deformation of density surfaces (neglecting the mostly tidal APE of the free surface). Another benefit of using the local APE is that one may distinguish between features in which water parcels have been displaced up or down relative to their rest depth. While this distinction would be meaningless for oscillatory features like internal waves, it clearly distinguishes the different ways APE′ is stored in coastal upwelling $\mathrm{APE}'_{\mathrm{up}}$ and estuaries $\mathrm{APE}'_{\mathrm{down}}$.

Acknowledgments. This work was supported by NSF OCE-0849622 and DOE DE-SC0006866 (PM), NSF OCE Postdoctoral Research Fellowship 1226406 (SNG), and NOAA NA09NOS4780180 (PM and SNG) as part of the Pacific Northwest Toxins (PNWTOX) project. The method for calculating geostrophic wind work was suggested by Leif Thomas.

REFERENCES

Austin, J. A., and J. A. Barth, 2002: Variation in the position of the upwelling front on the Oregon shelf. *J. Geophys. Res.*, **107**, 3180, doi:10.1029/2001JC000858.

Barron, C. N., A. B. Kara, P. J. Martin, R. C. Rhodes, and L. F. Smedstad, 2006: Formulation, implementation and examination of vertical coordinate choices in the global Navy Coastal Ocean Model (NCOM). *Ocean Modell.*, **11**, 347–375, doi:10.1016/j.ocemod.2005.01.004.

——, L. F. Smedstad, J. M. Dastugue, and O. M. Smedstad, 2007: Evaluation of ocean models using observed and simulated drifter trajectories: Impact of sea surface height on synthetic profiles for data assimilation. *J. Geophys. Res.*, **112**, C07019, doi:10.1029/2006JC003982.

Biton, E., and H. Gildor, 2014: Energy budget of a small convectively driven marginal sea: The Gulf of Eilat/Aqaba (northern Red Sea). *J. Phys. Oceanogr.*, **44**, 1954–1972, doi:10.1175/JPO-D-13-0220.1.

Carter, G. S., and Coauthors, 2008: Energetics of M_2 barotropic-to-baroclinic tidal conversion at the Hawaiian Islands. *J. Phys. Oceanogr.*, **38**, 2205–2223, doi:10.1175/2008JPO3860.1.

Cessi, P., N. Pinardi, and V. Lyubartsev, 2014: Energetics of semienclosed basins with two-layer flows at the strait. *J. Phys. Oceanogr.*, **44**, 967–979, doi:10.1175/JPO-D-13-0129.1.

Cushman-Roisin, B., and J.-M. Beckers, 2011: *Introduction to Geophysical Fluid Dynamics: Physical and Numerical Aspects*. 2nd ed. Academic Press, 875 pp.

Egbert, G. D., and S. Y. Erofeeva, 2002: Efficient inverse modeling of barotropic ocean tides. *J. Atmos. Oceanic*

Technol., **19**, 183–204, doi:10.1175/1520-0426(2002)019<0183:EIMOBO>2.0.CO;2.

Emery, W. J., and R. E. Thomson, 1998: *Data Analysis Methods in Physical Oceanography*. Elsevier, 634 pp.

Ferrari, R., and C. Wunsch, 2009: Ocean circulation kinetic energy: Reservoirs, sources, and sinks. *Annu. Rev. Fluid Mech.*, **41**, 253–282, doi:10.1146/annurev.fluid.40.111406.102139.

Floor, J. W., F. Auclair, and P. Marsaleix, 2011: Energy transfers in internal tide generation, propagation and dissipation in the deep ocean. *Ocean Modell.*, **38**, 22–40, doi:10.1016/j.ocemod.2011.01.009.

Geyer, W. R., and P. MacCready, 2013: The estuarine circulation. *Annu. Rev. Fluid Mech.*, **46**, 175–197, doi:10.1146/annurev-fluid-010313-141302.

Giddings, S. N., and Coauthors, 2014: Hindcasts of potential harmful algal bloom transport pathways on the Pacific Northwest coast. *J. Geophys. Res. Oceans*, **119**, 2439–2461, doi:10.1002/2013JC009622.

Haidvogel, D. B., H. G. Arango, K. Hedstrom, A. Beckmann, P. Malanotte-Rizzoli, and A. F. Shchepetkin, 2000: Model evaluation experiments in the North Atlantic basin: Simulations in nonlinear terrain-following coordinates. *Dyn. Atmos. Oceans*, **32**, 239–281, doi:10.1016/S0377-0265(00)00049-X.

Hickey, B., A. MacFadyen, W. Cochlan, R. Kudela, K. Bruland, and C. Trick, 2006: Evolution of chemical, biological, and physical water properties in the northern California Current in 2005: Remote or local wind forcing? *Geophys. Res. Lett.*, **33**, L22S02, doi:10.1029/2006GL026782.

Holliday, D., and M. E. McIntyre, 1981: On potential energy density in an incompressible, stratified fluid. *J. Fluid Mech.*, **107**, 221–225, doi:10.1017/S0022112081001742.

Kang, D., and O. Fringer, 2010: On the calculation of available potential energy in internal wave fields. *J. Phys. Oceanogr.*, **40**, 2539–2545, doi:10.1175/2010JPO4497.1.

——, and ——, 2012: Energetics of barotropic and baroclinic tides in the Monterey Bay area. *J. Phys. Oceanogr.*, **42**, 272–290, doi:10.1175/JPO-D-11-039.1.

——, and E. N. Curchitser, 2015: Energetics of eddy–mean flow interactions in the Gulf Stream region. *J. Phys. Oceanogr.*, **45**, 1103–1120, doi:10.1175/JPO-D-14-0200.1.

Lorenz, E. N., 1955: Available potential energy and the maintenance of the general circulation. *Tellus*, **7**, 157–167, doi:10.1111/j.2153-3490.1955.tb01148.x.

MacCready, P., 2011: Calculating estuarine exchange flow using isohaline coordinates. *J. Phys. Oceanogr.*, **41**, 1116–1124, doi:10.1175/2011JPO4517.1.

——, N. S. Banas, B. M. Hickey, E. P. Dever, and Y. Liu, 2009: A model study of tide- and wind-induced mixing in the Columbia River estuary and plume. *Cont. Shelf Res.*, **29**, 278–291, doi:10.1016/j.csr.2008.03.015.

Marsaleix, P., F. Auclair, J. W. Floor, M. J. Herrmann, C. Estournel, I. Pairaud, and C. Ulses, 2008: Energy conservation issues in sigma-coordinate free-surface ocean models. *Ocean Modell.*, **20**, 61–89, doi:10.1016/j.ocemod.2007.07.005.

Mass, C. F., and Coauthors, 2003: Regional environmental prediction over the Pacific Northwest. *Bull. Amer. Meteor. Soc.*, **84**, 1353–1366, doi:10.1175/BAMS-84-10-1353.

Pierce, S. D., J. A. Barth, R. E. Thomas, and G. W. Fleischer, 2006: Anomalously warm July 2005 in the northern California Current: Historical context and the significance of cumulative wind stress. *Geophys. Res. Lett.*, **33**, 2–7, doi:10.1029/2006GL027149.

Saenz, J. A., R. Tailleux, E. D. Butler, G. O. Hughes, and K. I. C. Oliver, 2015: Estimating Lorenz's reference state in an ocean with a nonlinear equation of state for seawater. *J. Phys. Oceanogr.*, **45**, 1242–1257, doi:10.1175/JPO-D-14-0105.1.

Scotti, A., and B. White, 2014: Diagnosing mixing in stratified turbulent flows with a locally defined available potential energy. *J. Fluid Mech.*, **740**, 114–135, doi:10.1017/jfm.2013.643.

——, R. Beardsley, and B. Butman, 2006: On the interpretation of energy and energy fluxes of nonlinear internal waves: An example from Massachusetts Bay. *J. Fluid Mech.*, **561**, 103–112, doi:10.1017/S0022112006000991.

Shchepetkin, A. F., and J. C. McWilliams, 2005: The Regional Oceanic Modeling System (ROMS): A split-explicit, free-surface, topography-following-coordinate oceanic model. *Ocean Modell.*, **9**, 347–404, doi:10.1016/j.ocemod.2004.08.002.

Sutherland, D. A., P. MacCready, N. S. Banas, and L. F. Smedstad, 2011: A model study of the Salish Sea estuarine circulation. *J. Phys. Oceanogr.*, **41**, 1125–1143, doi:10.1175/2011JPO4540.1.

Tailleux, R., 2013: Available potential energy and exergy in stratified fluids. *Annu. Rev. Fluid Mech.*, **45**, 35–58, doi:10.1146/annurev-fluid-011212-140620.

Thomson, R. E., S. F. Mihály, and E. A. Kulikov, 2007: Estuarine versus transient flow regimes in Juan de Fuca Strait. *J. Geophys. Res..*, **112**, C09022, doi:10.1029/2006JC003925.

Waterhouse, A. F., and Coauthors, 2014: Global patterns of diapycnal mixing from measurements of the turbulent dissipation rate. *J. Phys. Oceanogr.*, **44**, 1854–1872, doi:10.1175/JPO-D-13-0104.1.

Winters, K. B., and R. Barkan, 2013: Available potential energy density for Boussinesq fluid flow. *J. Fluid Mech.*, **714**, 476–488, doi:10.1017/jfm.2012.493.

——, P. N. Lombard, J. J. Riley, and E. A. D'Asaro, 1995: Available potential energy and mixing in density-stratified fluids. *J. Fluid Mech.*, **289**, 115–128, doi:10.1017/S002211209500125X.

Wunsch, C., and R. Ferrari, 2004: Vertical mixing, energy, and the general circulation of the oceans. *Annu. Rev. Fluid Mech.*, **36**, 281–314, doi:10.1146/annurev.fluid.36.050802.122121.

Young, W. R., 2010: Dynamic enthalpy, conservative temperature, and the seawater Boussinesq approximation. *J. Phys. Oceanogr.*, **40**, 394–400, doi:10.1175/2009JPO4294.1.

Zemskova, V. E., B. L. White, and A. Scotti, 2015: Available potential energy and the general circulation: Partitioning wind, buoyancy forcing, and diapycnal mixing. *J. Phys. Oceanogr.*, **45**, 1510–1531, doi:10.1175/JPO-D-14-0043.1.